

Experimental and Numerical Simulation of Restraining Forces in Gas Metal Arc Welded Joints

The restraining force due to gas metal arc welding has been investigated both numerically and experimentally

BY M. A. WAHAB, M. S. ALAM, M. J. PAINTER, AND P. E. STAFFORD

ABSTRACT. The gas metal arc welding process (a method of joining two metals by diffusion) is used to join metal in many industrial applications. Restraining forces arise from the nonuniform thermal field generated by welding. In this study, restraining force exerted during the welding process is calculated both numerically and experimentally. In numerical analysis, finite element software (*ANSYS*) has been used. In experimental analysis, a jig was designed and built that uses load cells to measure the force required to restrain two mild steel plates (base plate) while they are being welded by an automatically controlled welding robot. After checking for reliability, tests were carried out to determine the effects of various welding speeds and heat inputs on the restraining forces. The results showed that welding speed has little effect on the restraining force but by increasing heat input, restraining forces increase significantly. The most relevant and useful information on the effects of the welding conditions is derived from the slope of the graph of the force vs. the distance traveled in time. The finite element predictions of restraining force due to various welding conditions produce similar trends and the slopes as the experimental results.

Introduction

The development of welding technology to its present state is one of the most significant manufacturing achievements in this century. Power plants, super tankers,

pipelines, and ground vehicles are just a few examples of structures that are critically dependent on welding operations. Postweld distortion, residual stresses, and altered microstructures are all undesirable effects of welding operations that cost industry millions of dollars each year to prevent or to correct (Refs. 1, 2). There has been an international effort to find suitable solutions to this postweld distortion, which is the change in shape experienced by a structure as a result of the fusion welding process. In fusion welding processes, local expansion, contraction, and volume change from phase transformations lead to nonhomogeneous plastic deformation and the generation of residual stress fields (Refs. 3–5). There has been a significant amount of research on the measurement of residual stress and distortion.

A significant contribution has been reported on the topics of residual stress and distortion by Masubuchi, who compiled recent findings in book form in the international series on material science and technology (Ref. 6). These methods either measure free-distortion of an unrestrained plate or residual stress of a restrained plate after postweld cooling. Hideyuki and Akitake (Ref. 7) developed a method of modeling the draw bead effect as well as a method of estimating the restraining force as a function of the direction of drawbead line and geometry. They developed a specific apparatus to measure the drawbead force under a different clearance and different sheet sliding directions against the draw bead line.

They also simulated the draw bead forming process to obtain a general understanding of the draw bead effect.

Jang and Lee (Ref. 8) proposed a method for predicting the welding deformation of large structures. The method uses both inherent strain theory and experimental results combined with the finite element method for accurate and efficient analysis. In the inherent strain theory, residual plastic strain due to welding is defined as the inherent strain. Assuming the inherent strain is the initial strain, welding deformation can be easily calculated by elastic finite element analysis, omitting the complicated thermal elastic-plastic finite element analysis. Ueda and Ma (Ref. 9) described inherent strain for a fillet joint using a series function. Based on the series function, a simplified distribution pattern for inherent strains was derived. Jang and Seo (Ref. 10) estimated the inherent strain region and represented the inherent strain as a function of the mechanical melting temperature and the degree of restraint. The degree of restraint represents the level of resistance against the thermal deformation of the welding region. The degree of restraint of a stiffened panel was determined from the analogy of the bar-spring model in the case of the simplified analysis model.

Murakawa et al. (Ref. 11) used a simplified analysis model to obtain the inherent strain. They represented the inherent strain as a function of the highest temperature and degree of restraint. However, this method has limitations when applied to complicated structures. Seo and Jang (Ref. 12) calculated the deformation of a large structure using the unit loading method to obtain the degree of restraint. Tsai et al. (Ref. 13) studied the distortion mechanisms and the effect of welding sequence on panel distortion. In their study, distortion behaviors, including local plate bending and buckling as well as global girder bending, were investigated using the finite element method. It was found that buckling doesn't occur in

M. A. WAHAB and M. S. ALAM are with Department of Mechanical Engineering, Louisiana State University, Baton Rouge, La. M. J. PAINTER is with the Commonwealth Scientific & Industrial Research Organization — Division of Manufacturing Science & Technology (CSIRO-CMST), Adelaide Lab., Adelaide, Australia. The late P. E. STAFFORD was with Department of Mechanical Engineering, University of Adelaide, Adelaide, Australia.

KEYWORDS

Gas Metal Arc Welding
Restraining Force
Finite Element Method
Butt Joint

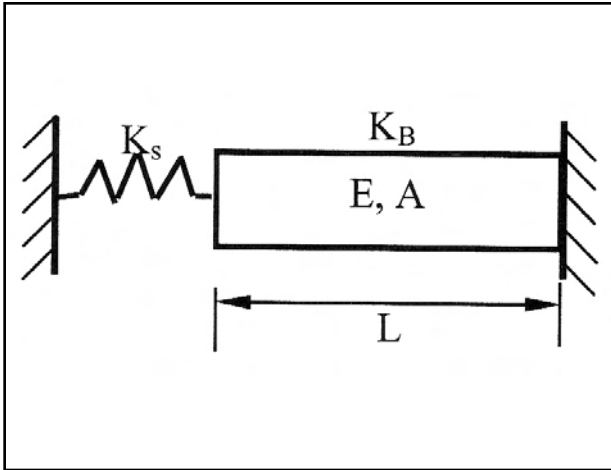


Fig. 1 — A simple elastic-plastic model of welding.

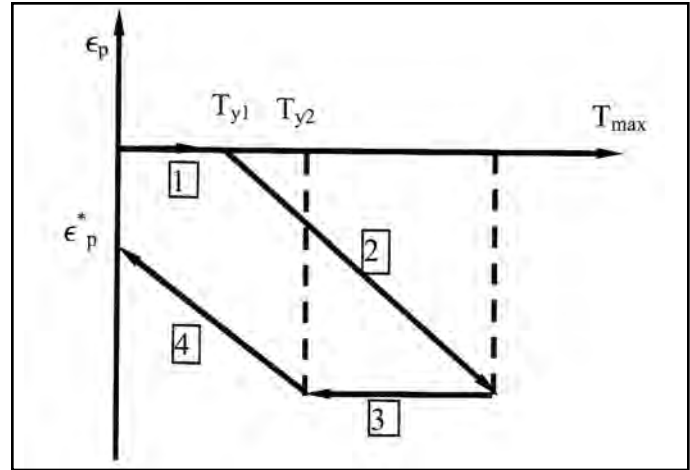


Fig. 2 — Thermal history of plastic strain during welding.

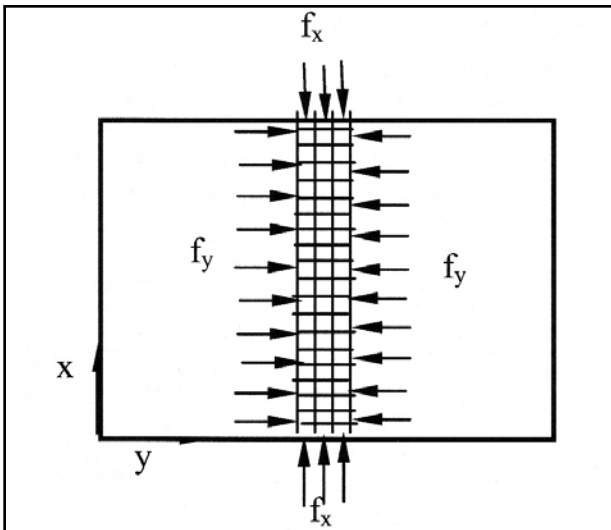


Fig. 3 — Equivalent loads of inherent strain.

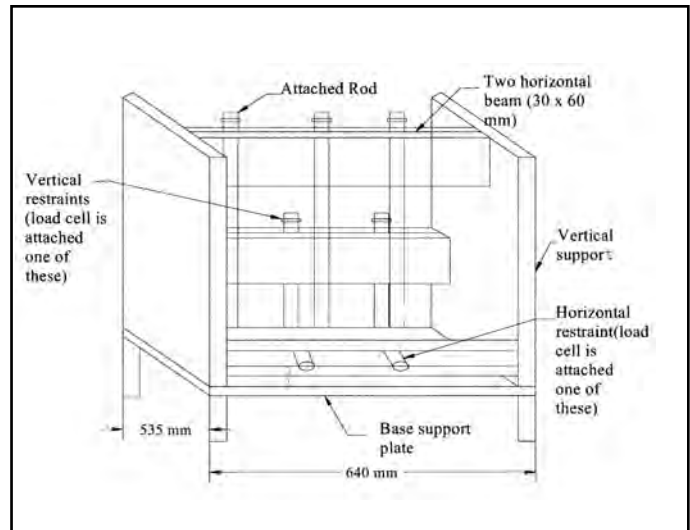


Fig. 4 — CAD drawing of the jig.

structures with a skin-plate thickness of more than 1.6 mm unless the stiffening girder bends excessively. Warping is primarily caused by angular bending of the plate itself. The joint rigidity method (JRM) was found to be effective in determining the optimum welding sequence for minimum panel warping.

For experimental weldability studies, taking into account predominantly the real structural effects on shrinkage restraint, the instrumented restraint cracking (IRC) test has been developed by Hoffmeister et al. (Refs. 14, 15). The IRC test has the capability of continuous registration of the reaction forces and moments during welding and subsequent cooling. The test has been extensively applied to avoid cold cracking of linear welds and to investigate the effects of heat input as well as pre- and postheating on the reaction force, and stress buildup during

cooling after welding of specifically restrained joints.

Bretz and Hoffmeister (Ref. 16) investigated the effects of heat input and hydrogen partial pressure of the gas tungsten arc welding (GTAW) process without welding wire and of restrained conditions in the instrumented restraint cracking (IRC) test on hydrogen-induced cracking for weld metals (StE 380, 15 NiCrMo, 10 6 (HY 80), and 12 Ni 19). In their study, the weld metals were fused exclusively from the roots of the plate materials. They found that the continuously measured combined nominal stresses transverse to the welds are strongly dependent on the transformation stress-release prior to cold cracking of the respective weld metals, and they also found that the higher restraint increases the nominal stresses. They found that the critical heat inputs for prevention of hydrogen weld metal crack-

ing are increased with the given restraint conditions, hydrogen potentials, and carbon contents of the weld metal (12 Ni 19), revealing no fracture conditions. Potente et al. (Ref. 17) investigated the development of inherent stresses arising during welding by the drilled-hole technique and finite element method. A rectangular plate and an actual rear car-light geometry were investigated. In both cases, there was a clear correlation between the inherent stresses induced and the welding parameters. In addition, by heating the parts prior to welding, it was possible to reduce the level of inherent stresses in the component and this way it was possible to make a contribution toward the avoidance of stress cracking. Boellinghaus and Kannegiesser (Ref. 18) studied the effect of filler material selection and shrinkage restraint on strain buildup in component welds. They considered two cases, sub-

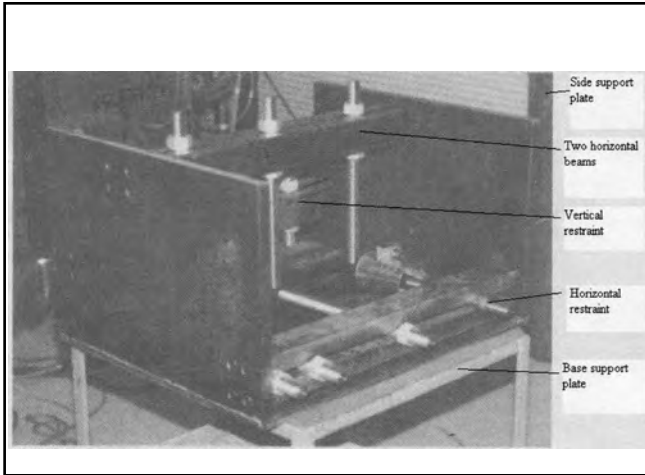


Fig. 5 — Original picture of the jig.

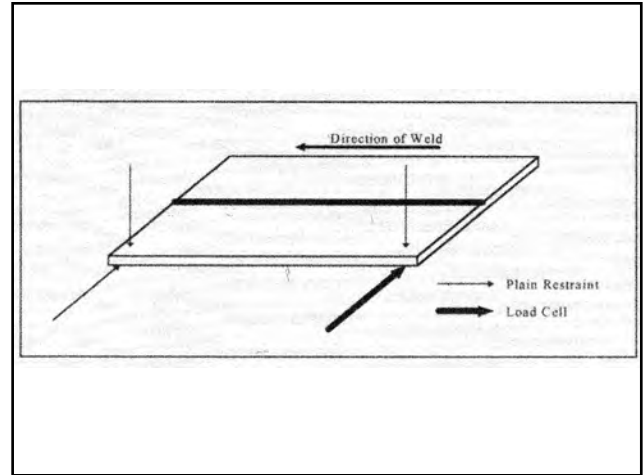


Fig. 6 — Position of load cell and restraint for side and top of plate.

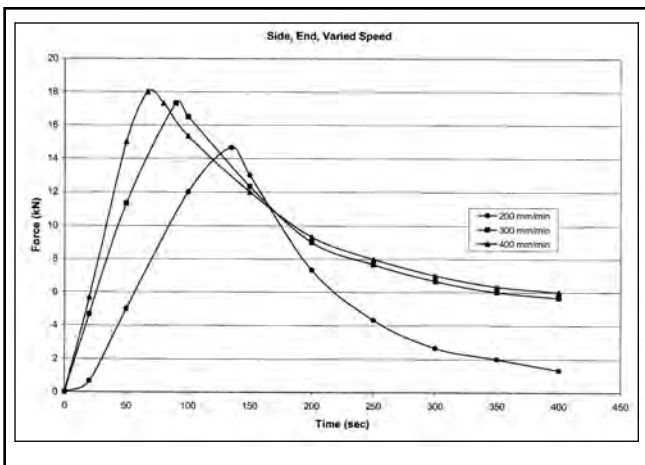


Fig. 7 — Variation of restraining forces with weld speed at constant heat input of 1 kJ/mm (1 kN = 224.81 lb_f, 1 kJ = 0.95 Btu).

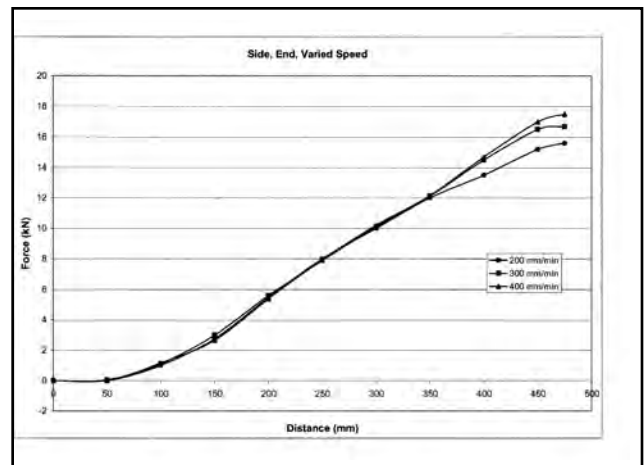


Fig. 8 — Variation of restraining forces with distance for varied speeds.

merged arc welded butt joints of structural steel plates and orbital GTAW of supermartensitic stainless steel tubular joints. They found that in both cases, the forces and residual stresses transverse to the weld could be significantly reduced by selecting overmatching filler materials. Kanngieber et al. (Ref. 19) investigated the effect of weld metal strength and welding conditions on reaction forces and stress distribution of restrained components. In order to achieve a closer insight into the structural effects, component weldability tests were performed by on-line monitoring of the reaction forces and moments. In particular, the effects of different values of the base material and weld metal strength on the reaction force and stress buildup transverse to the welding direction were studied at a specific structural restraint. They found that the final reaction force

and also the reaction stress level in the multilayer butt-joint welds decreases with overmatch of the weld metal. Reaction forces and moments built up during welding and subsequent cooling were measured in a specifically designed large-scale testing facility. Residual stresses were measured by the hole-drilling technique after cooling of the specimens in the restrained as well as in the relieved (unrestrained) condition.

To the best of the authors' knowledge, there are few works (as mentioned earlier) found in the literature that have indicated measurement of restraining forces, and further investigation may enhance this field of study. The major objective of this current research is to simulate the restraining force of gas metal arc welded plate both experimentally and numerically. Interesting new results have been observed from this investigation.

Mathematical Relation of Restraint Forces

In the welding process, the heat input around a weld joint causes a nonuniform temperature distribution and thermal stress. As a result, the plastic strain remains around the weld bead and permanent deformation occurs after welding. The plastic strain that causes the welding deformation is defined as the inherent strain (Ref. 8). In general, the inherent strain caused by welding has six components according to their directions. However, in the case where a plate has a large length/thickness ratio, only two components ϵ_{px}^* and ϵ_{py}^* are dominant, where ϵ_{px}^* and ϵ_{py}^* are inherent plastic strain in x and y directions, respectively.

The inherent strain distribution and the restraining force can be formulated

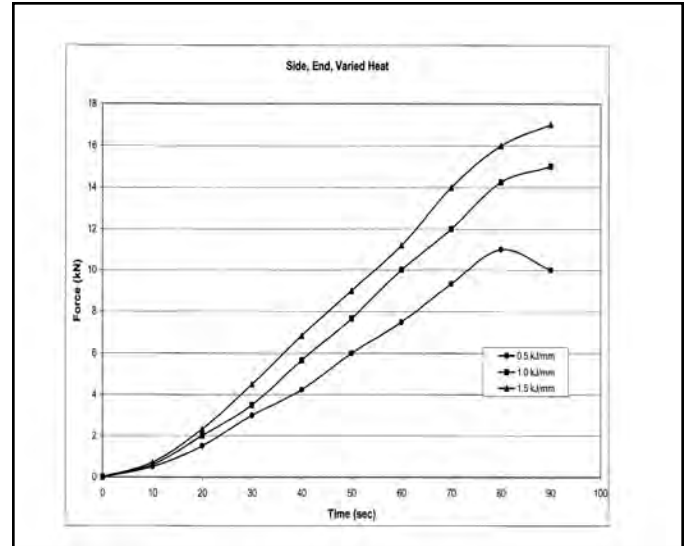
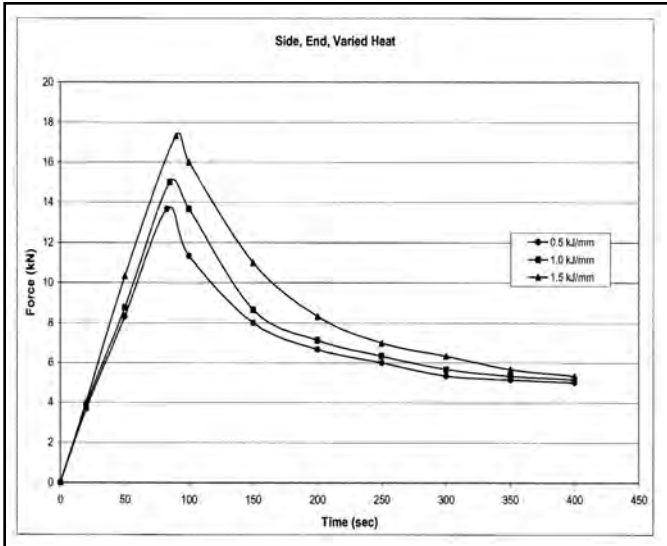


Fig. 9 — Variation of restraining forces with heat input at constant speed (300 mm/min) (1 kN = 224.81 lb_f, 1 kJ = 0.95 Btu).

Fig. 10 — Detail of restraint force rise while welding (side, end, and varied heat, first portion of Fig. 9).

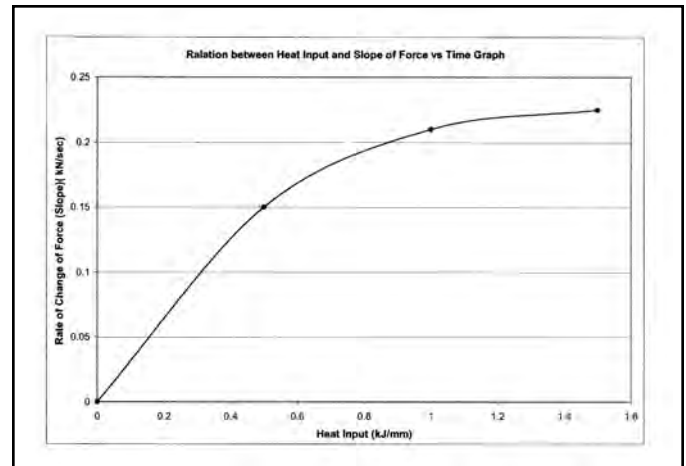
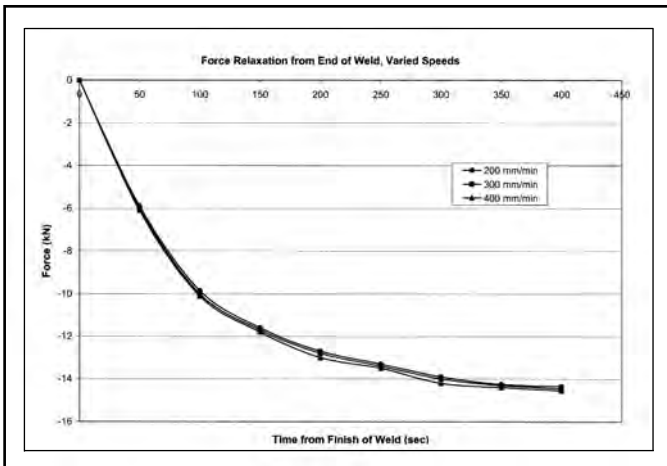


Fig. 11 — Force relaxation over time (second portion of Fig. 9) when arcs are removed.

Fig. 12 — Heat input and slope of force vs. time graph.

using a simplified thermal elastic-plastic analysis model as shown in Fig. 1. The welding region, where the inherent strain occurs, can be modeled as a bar and a spring. The bar element has stiffness K_B , modulus of elasticity E , cross-sectional area A , and length L . The spring element has stiffness K_s .

The thermal history of the inherent strain according to the temperature change of the bar can be divided into four steps, as shown in Fig. 2. After all the thermal history, the compressive plastic strain remains as an amount ϵ_p^* . The magnitude of residual plastic strain can be calculated from the total strain, the stress-strain relation, and the equilibrium equation of a bar-spring system.

$$\text{Total strain} \quad \epsilon = \epsilon_{\text{ther}} + \epsilon_c + \epsilon_p \quad (1)$$

$$\text{Stress-strain relations} \quad \sigma = E\epsilon_c \quad (2)$$

$$\text{Equilibrium equation} \quad F_B = F_S \quad (3)$$

$$\text{The restraining force} \quad F_s = K_s \epsilon_p^* L \quad (4)$$

where ϵ is total strain, ϵ_{ther} thermal strain, ϵ_c elastic strain, ϵ_p plastic strain, σ stress, E modulus of elasticity, F_B internal force of the bar element, and F_S internal force of the spring.

In the finite element model, the equivalent restraint forces can be obtained by using the inherent strain. All types of equivalent loads are shown in Fig. 3. The restraining force f_{yi} and f_{xi} can be found

using Equations 5 and 6

$$f_{yi} = \frac{AE}{l} \sum_{j=1}^{N_i} \epsilon_{pyj}^* l_j \quad (5)$$

$$f_{xi} = \frac{AE}{l} \sum_{j=1}^{N_i} \epsilon_{pxj}^* l_j \quad (6)$$

where l_j is the finite element length. The total equivalent transverse and longitudinal forces can be calculated using Equations 7 and 8, respectively.

$$f_y = \sum_{i=1}^n f_{yi} \quad (7)$$

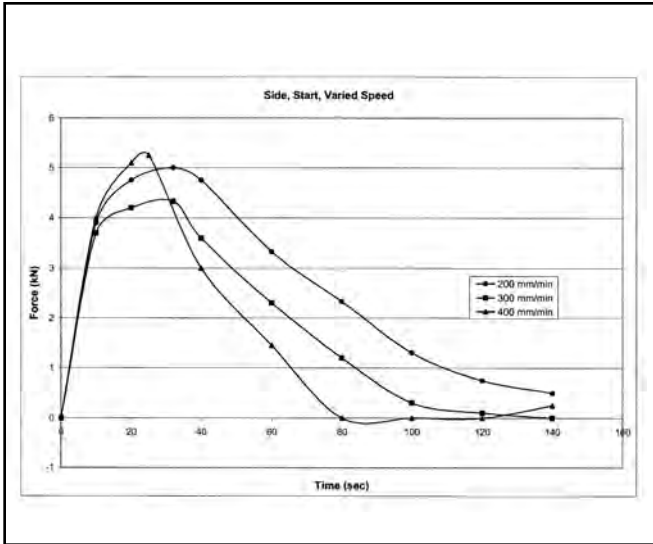


Fig. 13 — Variation of restraining forces with speed for side and start locations.

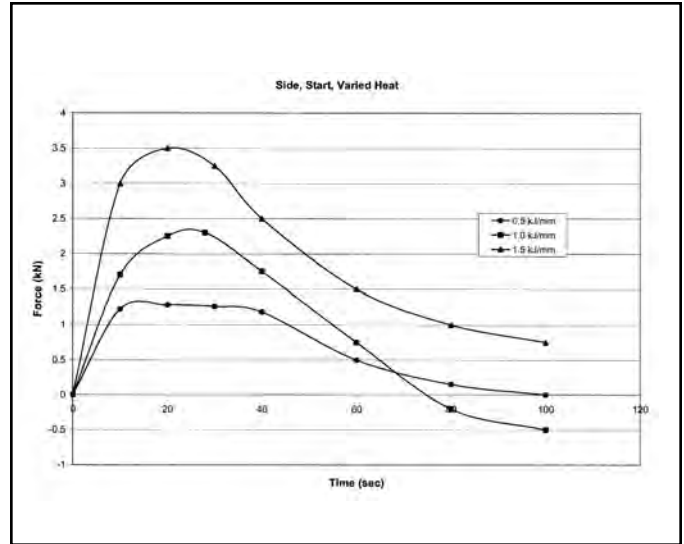


Fig. 14 — Variation of restraining force with heat input for side and start locations.

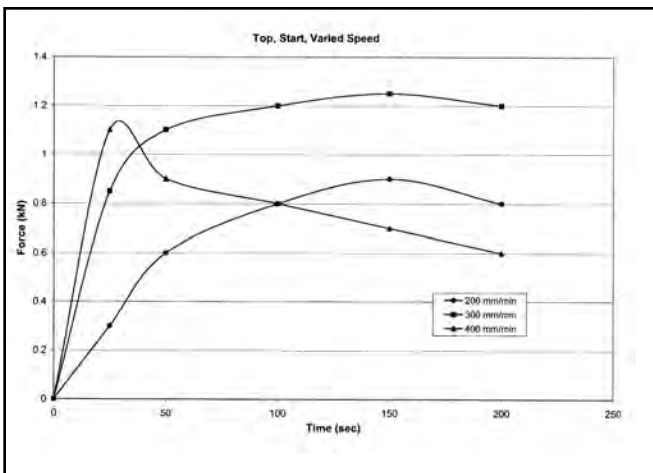


Fig. 15 — Variation of restraining force with weld speed for top and start locations.

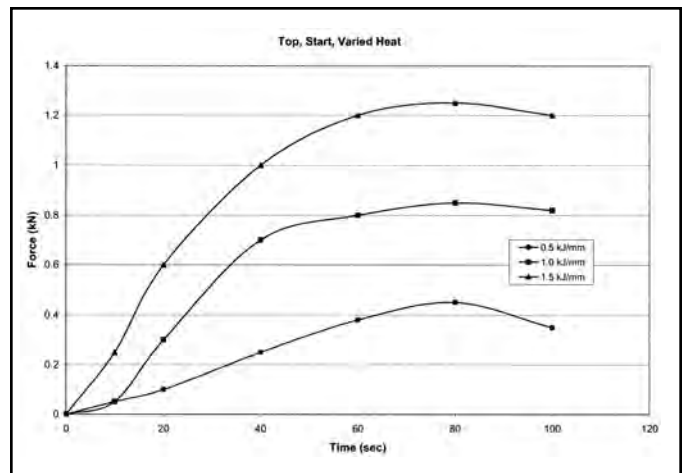


Fig. 16 — Variation of restraining forces with heat input for top and start locations.

$$f_x = \sum_{i=1}^N f_{xi} \quad (8)$$

Experimental Procedure

Design

To generate the experimental data, a jig was designed and built — Figs. 4, 5. The aim of the jig was to hold two steel plates in position while the butt joints were welded and to measure the restraining forces in position. The jig has a flat bed that the plates sit on and restraints mounted to load cells that measure the restraining force on the top and side. The jig was designed to comply with the following constraints:

- To hold two hot-rolled mild steel plates, 10 × 100 × 500 mm (0.4 × 4 × 20 in.);
- To allow measurement of restraining forces typically in the vertical and horizontal directions during simple butt-joint welding;
- To allow access to the gas metal arc welding robot;
- To allow flexible placement of the restraint positions (restraint can be placed in many positions).

To measure the restraining forces (transverse (y) and vertical directions (z)), it is necessary to use some suitable force-measuring device. The two types of force measuring devices available are strain gauge and load cell. For ease of interpretation of output and simplicity of design, load cells were selected.

As a result of thermal expansion and the application of restraints, the welded

steel plates will shrink in the direction perpendicular to the direction of the weld. The jig was designed to measure only in compression force (when two plates are welded along the centerline and edges are kept restrained, due to expansion of the weld plate compression force exerted on the restraint), which includes the restraining forces for expansion of the plate and contraction up to zero load (0.0 kN) condition.

Configuration

The aim of the design of the jig (Figs. 4 and 5) is to hold the load cells against the plates so that they can prevent the plates from distorting and measure the restraining forces. The load cells are attached to studs, which tighten against slotted beams above and to the side of the plates. An im-

Table 1 — Welding Conditions for Constant Speed but Varied Heat Input

Current (A)	Voltage (V)	Heat Input (KJ/mm)	Speed (mm/min)
124	20	0.5 (12 Btu/in.)	300 (12 in./min)
232	23	1.0 (24 Btu/in.)	300 (12 in./min)
278	27	1.5 (36 Btu/in.)	300 (12 in./min)

Table 2 — Welding Conditions for Constant Heat Input, Varied Speed

Current (A)	Voltage (V)	Heat Input (KJ/mm)	Speed (mm/min)
228	23	1.5 (36 Btu/in.)	200 (8 in./min)
278	27	1.5 (36 Btu/in.)	300 (12 in./min)
334	31	1.5 (36 Btu/in.)	400 (16 in./min)

Table 3 — Welding Parameters

Base Plate	Mild steel plate (ASTM A-36), yield strength 280
Welding Wire	Auto craft LW1 (yield strength 390 MPa) type welding wire of 1.2 mm (0.05 in.) diameter
Gas	Argon with 1.5% Oxygen
Air Temperature	18–25 degrees Celsius
Electrode Extension	16 mm (0.63 in.) (except 0.5 kJ/mm: 11 mm [0.45 in.]

portant consideration for the design of the jig is to make sure that the bed and restraint supports (both vertical and transverse directions) are stiff enough to resist buckling, and uncontrolled or excessive deflections are minimized. If either the bed or restraint supports deflected significantly, the results would become inaccurate. The layout of the jig consists of two end plates with the bed and restraint supports (both horizontal and vertical) lying in between them — Fig. 4. Because the two plates being welded were identical, the restraining forces experienced by both plate edges are the same. For this reason, the jig is designed only to restrain one plate with load cell. The plate restrained with load cells will be referred to as the measured plate. An important part of the design of the restraint supports was to make them versatile enough to restrain the plates with any number of restraints in any position. This was achieved by the slots in the mild steel beams, which allow the studs to slide to any position. A flat bed is needed to keep the two pieces of steel plate absolutely flat while being welded. As well as being flat, the bed must be stiff enough to prevent any noticeable deflection. To accommodate this design consideration, the backbone of the bed is four 20 × 50 mm steel bars that join to each endplate. Two of these bars lie under each of the test plates, one directly under the line

of top restraint, another 10 mm to the side of the weld bead. This leaves a 20-mm-wide gap under the weld. A piece of wood is placed in the bottom of the gap to protect the jig in the event of the weld pool falling through the plates. Underneath the bars and the end plates, there is a 640 × 535 × 10-mm steel base plate to support the whole structure.

Instrumentation and Testing

The data was collected with two load cells connected to a load cell amplifier with the output to a data logger. A 20-kN (4496-lbf) load cell was used in low force position on the jig. The 10-kN (2248-lbf) load cells (Tokyo Sokki CLP 10B) were calibrated by compressing them in an MTS testing machine and charting the output voltage from the amplifier against the measured load on the MTS. The restraints could be tightened against the plate with a compressive force, called preloading. The effects of preloading had to be determined to find the best experimental procedure and ensure that the experiments could be reliably repeated. A large preload greatly decreased the restraining force before and after the peak force value. This can be explained by the restrained expansion and free contraction model described by Cornu (Ref. 20). When the stress of the base metal exceeds the yield strength of the material in the high-temper-

ature region near the weld, the restraining force is relieved by plastic deformation. In the case of a large preload, the preload (initial load) is also relieved by plastic deformation. This results in greater shrinkage and the restraining force drops. For the force values taken from the side positions to be true, there must be no sideways force resisted by the top restraints. Increasing the force on the top of the plates did not reduce the force measured by a load cell on the side of the plate.

Test Procedure

The aim of the experiments is to gain an understanding of what factors influence distortion by undertaking two main sets of experiments, varying one parameter at a time. As this research aim was to look at the overall trends for each parameter rather than calculation of the effects of a small change, only three samples were taken, from the upper, central, and lower bounds of what may be used in commercial practice.

Two restraints on each of the tops and edges of each plate were used. This helps to understand the results better than those of three restraints tried earlier. This gives a total of four positions from which data will be collected: top start, top end, side start, and side end — Fig. 6.

To conduct an experiment with the jig, the following steps were taken:

1. Two steel plates are placed on the bed and pushed against the end stops.
2. The load cells and other supports are placed in their positions and tightened to about 1 kN (224.81 lbf).
3. The load cells are connected to the amplifier and the amplifier is set to the appropriate gain setting.
4. The amplifier is connected to the data logger and the appropriate data is entered into the data logger.
5. The robot is programmed according to the desired welding conditions.
6. Data from the data logger can be loaded directly into MS® Excel and analyzed.

Welding Conditions

The first sets of experiments were carried out keeping the welding speed constant and changing the heat input. The range in heat inputs covered spans from the minimum to maximum, which could be used on the 10 × 100-mm (0.4 × 4-in.) mild steel.

The next set of experiments examined the effect of applying the same heat input at various speeds. The values for various parameters (variables) for different welding conditions (constant speed, variable speed) are given in Tables 1–3.

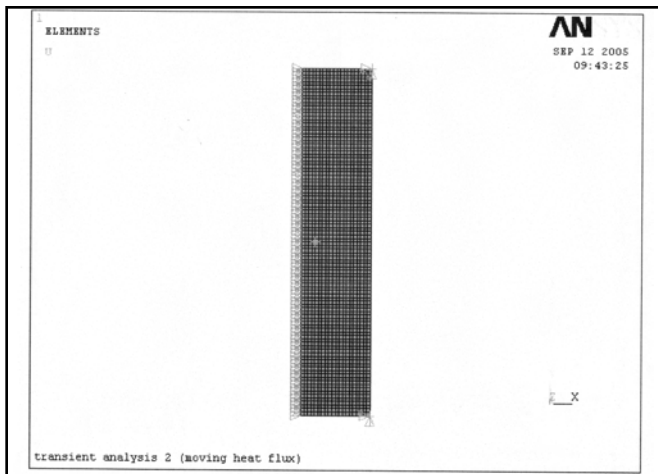


Fig. 17 — 3-D FEM weld model with mesh and boundary condition (500 × 100 × 10 mm).

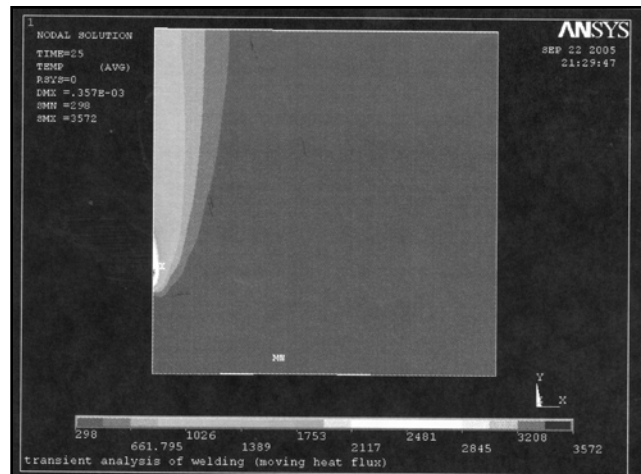


Fig. 18 — Finite element model showing moving heat flux.

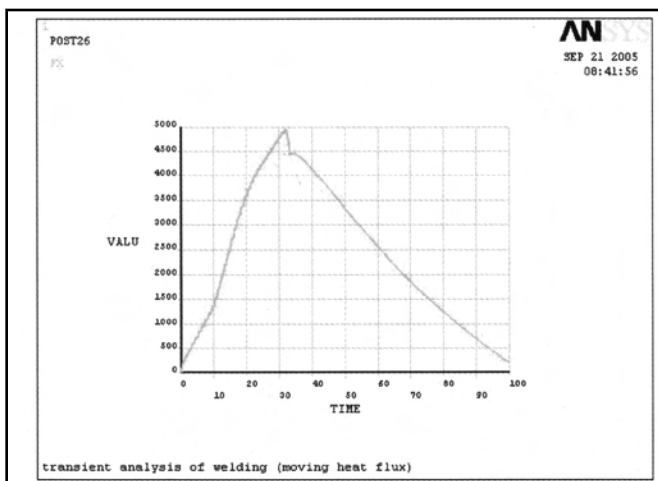


Fig. 19 — Restraining force found from Ansys postprocessing for side, start position with weld speed 300 mm/min and heat put 1 kJ/mm.

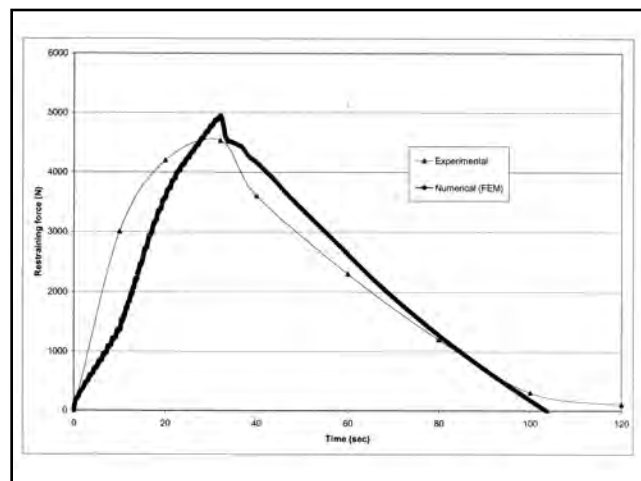


Fig. 20 — Comparison of predictions with experimental result for side, start position with weld speed 300 mm/min and heat put 1 kJ/mm.

Edge Preparation

A square butt joint was selected for the experiments described previously because it allows greater flexibility in welding conditions. The jig was designed to be used for a single pass, and the influence of the weld bead shape on the restraining forces is more visible in a square butt joint because depth of penetration and width of weld bead depend directly on the welding conditions.

Experimental Results and Discussions

Side, End of Weld

The variation of restraining force over weld speed is shown in Fig. 7. It is seen that as the speed increases, the peak occurs earlier and at a higher force. The reason for the peak occurring earlier is because as the speed increases, the weld finishes ear-

lier. The peaks occur at the finish of the weld in all cases and this is shown by the black line, which is drawn where the welding current drops to 0.0 ampere for each weld. Further, the linear rise in force starts at the same position for all of the welding speeds. The delayed start is because the weld metal is initially (when drop on bead) liquid and, after solidification, it takes time to cool and expand (to attain the surrounding temperature, the base plate expands).

An easier, graphical way to understand this behavior uses a distance scale rather than a time scale — Fig. 8. This has all of the welds starting and ending at the same position on the x-axis and only shows the force while welding is happening. This plot shows that the restraint force is independent of speed for most of the graphs and only gains a dependence on speed in the region close to the restraint. As the weld gets closer to the restraint, the graphs

lose linearity with the slowest weld losing linearity first and the fastest last. This indicates that at any welding speed, the graph will be linear and any further increase in speed will not affect the restraining force. The linear rise in restraining force with distance indicates that the maximum force reached is a linear function of the length of the welded plates. So as a means of comparing two alternative welding processes, the slope of the linear part of the graph would be more useful.

Figure 9 shows the restraining forces for varied heat input but constant speed. As a means of comparing Fig. 9 with Fig. 7, the graph for 1.5 kJ/mm (36.2 Btu/in.) and 300 mm/min (12 in./min) is the same on both graphs. Figure 9 has four distinct sections that will be considered separately. These are a flat heating time, a linear rise, a nonlinear rise, and force relaxation. To make the first three sections easier, Fig. 10 is plotted for the time from the start to the

end of the weld and Fig. 11 is plotted for force relaxation. On this graph (Fig. 10), the flat heating time is clearly visible. The heating time is the same for all three heat inputs, which indicates that it is independent of heat input. The linear rise starts at the end of the heating zone and extends to the nonlinear zone near the end restraint. This is the most important part of the graph because the slope of the linear section gives a direct means of comparison of the effect of different heat inputs. After the arc cut-out, the force against the restraint relaxes with time — Fig. 11. The result shows that the force relaxation is a function of time that is affected neither by welding speed nor the restraining force at the end of the weld. It may be said that the relaxation of the restraining force during cooling is controlled by the deformations at stress level above the yield stress. The stress relaxation is simply the contraction of the welded plates with no plastic deformation. The fact that the contractions for all three welding speeds are the same indicates that all three welds must have undergone the same deformations in the expansion stage, and therefore have the same internal structure. This indicates that the departure from linearity of the force-distance curve resulting in a lower peak force has little effect on the deformation of the plate, which reinforces the idea that the slope of the curve is more important than the peak force.

For a clear comparison of the effects of heat input on restraining force, Fig. 12 shows the slope of the force-time curve plotted against heat input. This graph shows that the relationship is certainly nonlinear, but only has three data points so it cannot be conclusive at this stage. This graph can be used as a rough guide as to what the slope of the linear part of the force-time graph will be. It should be mentioned once again that the slope of the force-time graph is dependent on the shape and size of the two plates being welded and therefore the numbers presented in this paper cannot be applied directly to other sized plates without investigating further.

Side, Start

The load cell position at the start of the weld (Fig. 13) shows the restraining force required to restrain against thermal expansion only. Because the weld starts at this restraint, there is no initial force against the restraint. The first noticeable feature of this graph is that the restraining force rises from the instant the arc is struck, unlike the restraining force at the end of the plate. While the graphs are rising, they have approximately the same shape and peak at nearly the same place. This is because the heat input is the same

and the weld is deposited nearly the same amount. Regardless of speed, the rate of increase of force in the first few seconds is independent of time.

The variation of restraining force over varied heat is shown in Fig. 14. When the heat input is increased, the restraining force at the start of the weld is increased. Because of the poor resolution of the data logger for this set of data, an earlier set is shown on the graph, which was recorded with the x-y plotter. The weld for this graph was about 50 mm (2 in.) shorter than the welds discussed previously, but this should have no effect on the restraining force near the start of the weld. The graph shows clearly the rise in restraining force with increased heat. For all heat inputs, the peak occurs in about the same place, and by the end of the weld, the restraining force has decreased to about 0.0 kN.

Top, Start of Weld

There was little variation of the maximum force measured at the start and end of the weld for the same welding conditions, and therefore the discussion will concentrate at the start of the weld. This differs from the side of the plate where the restraining force is about three times larger at the end than the start. The variation of restraining force for the top of the plate, at the start of welding, and for variable speeds is shown in Fig. 15. There are two effects on the restraining force from welding speed. First, the force increases at a greater rate with increased welding speed, and second, the maximum restraining force increases with increasing welding speed. The steeper slope of the graph with increased force is because the faster weld finishes earlier. The first few seconds of the weld show instability because the restraining force varies between positive and negative with no clear pattern. This is especially evident on the graph for 200 mm/min (8 in./min). An interesting result is that the force for the 400 mm/min (16 in./min) graph starts to decrease before the weld is finished (63 s) while the 300 (12 in./min) and 200 mm/min (8 in./min) welds increase slowly until the weld finishes (90 and 135 s, respectively).

The variation of restraining force for the top of plate, start of weld at varied heat is shown in Fig. 16. The graph shows that increasing the heat input increases the restraining force. Both the slope of the graph and the maximum force reached increase as heat input increases. The relationship between heat input and restraining force is approximately linear, which means doubling the heat will double the peak restraining force. Because the fusion area increases with an increase of heat input, the restraining force increases. The instability of the first few seconds of the

weld increases with the decreasing welding speed.

Finite Element Model (FEM) and Analysis

A 3-D FEM model (Fig. 17) of a square butt-joint weld in a steel specimen of dimensions (500 × 100 × 10 mm [20 × 4 × 0.4 in.]) has been created using the authors' written *Ansys* code. For symmetry only half of the specimen has been considered for modeling and analysis. It is assumed that only convection occurs on the surface of the specimen and conduction occurs within the specimen. Convection describes the effect of temperature gradients between the post-weld plate surfaces and the room temperature of the surrounding air (assumed to be 30°C from the literature (Ref. 21)). In this case, it has been assumed that the plate surface-temperature changes due to the combined effects of two conditions, namely, 1) conduction within the specimen, and 2) convection from the specimen surface-temperature to the surrounding-air temperature. The temperature within the specimen changes from weld pool to the location away from the weld pool due to conduction.

The temperature-dependent material properties (i.e., modulus of elasticity, thermal conductivity, coefficient of specific heat, modulus of thermal expansion, Poisson's ratio, yield stress, tangent modulus, etc.) of base and weld materials were collected from the work of Henrik (Ref. 21) for various temperature conditions and have been applied to the model. A moving heat flux method is used in the transient heat transfer analysis — Fig. 18. The magnitude of the heat flux is determined from the heat input, welding speed, and thickness of the plate. For a set of welding parameters (i.e., voltage 23 V, current 232 A, welding speed 5 mm/s, arc efficiency 93.7%, and plate thickness of 10 mm), the magnitude of heat flux is calculated as $100E6 \text{ J/m}^2$ (voltage × current × arc efficiency / (weld speed × thickness)). This heat flux is applied as a surface elemental load from one end of the plate to the other, using a “do-loop” command. After finishing one increment of the “do-loop,” the previous heat flux is deleted and another heat flux (the same amount) is applied to the next element. The temperature constraints from the elements of the base material and weld materials are removed, which will allow the base metal to contract or expand freely. In the FE model, “Solid5” elements are used that have the capability of treating both conduction and convection conditions. The convection heat transfer coefficient for all external surfaces was assumed to be 100 W/m²/°C (2.152 Btu/min/in.²/°F) and the temperature of the surrounding air was 30°C (86°F) and these values are assumed from the work of Hen-

rick (Ref. 21). In transient analysis, the convective heat transfer is applied as a surface load using the authors' written *Ansys* code. The *Ansys* command "SF" is used for applying surface load and "CONV" is used to represent type of surface load. The convective heat transfer coefficient and the ambient temperature are also mentioned in the same command line.

The restraining force is found from fixing the edge nodes at the start and end positions and the reaction forces of the fixed nodes give the restraining forces.

FEM Results and Discussions

The restraining force for the side and start positions found in the *Ansys* analysis is shown in Fig. 19. The restraining forces increase with increase of time. Due to thermal expansion the volume of weld metal increases. Hence the restraining forces due to the expansion of weld metal increases with time, but when welding has been completed, the metal contracted due to the conduction and convection, and consequently, the restraining force decreases. For validation, the prediction has been compared with the experimental results shown in Fig. 20 for the side and at the start of the plate condition. The location and the magnitude of the maximum force for both experimentally obtained values and numerical results occur very close to each other and only slight variation occurs in the magnitudes. This slight variation (7%) in the magnitude of the peak force may be due to the change in actual material properties for both cases (experimental and prediction). Furthermore, the convective heat transfer coefficient that has been used in the numerical modeling may be slightly different from the actual experimental case and, accordingly, it can be concluded that the predicted results are within the acceptable ranges.

Conclusions

1. For a given heat input, the restraining force will be the same as a function of distance except close to the end of the plate while it is being welded, regardless of welding speed.

2. For a given heat input, the force relaxation (up to 0.0-N forces) after welding will have the same shape regardless of welding speed and maximum restraining forced reached.

3. Decreasing welding speed makes the force vs. distance graph depart from linearity earlier.

4. Increasing the heat input increases the slope of the force vs. time graph and the maximum restraining (reaction) force.

5. The slope of the force vs. time graph gives a better indication of the effects of the

welding conditions than maximum restraining force.

6. The restraining (reaction) force for the top of the plate increases with increased welding speed.

7. The restraining force for the top of the plate increases with increased heat input.

Acknowledgments

The experimental work described in this paper was undertaken as a part of a joint research project of the University of Adelaide, Australia and Commonwealth Scientific and Industrial Research Centre-Adelaide's Division of Manufacturing Science & Technology (CSIRO-CMST), Australia, and Louisiana State University, Baton Rouge. The authors gratefully acknowledge the help received from the late Peter E. Stafford in crucial experimental design, fabrication, and experimental data collections of this research. The research work is dedicated to his memory, who brought forward significant insight into this work through his dedication, scholarship, and perseverance. The numerical work was supported by the Louisiana State Economic Development Grant, Louisiana State University's Faculty Research Grant 2003-2004, and the funds from the Mechanical Engineering Department at Louisiana State University.

References

1. Bachorski, A., Painter, M. J., Smailes A. J., and Wahab, M. A. 1999. Finite element prediction of distortion during gas metal arc welding using shrinkage volume approach. *J. of Mater. Process. Tech.*, 92-93: 405-409.
2. Smith, S. D. 1994. A review of numerical modelling of fusion welding for the prediction of residual stresses and distortions. *TWI Journal* 3(4): 440-503.
3. Wohlfart, H., and Zhang, F. 1994. Experimental evaluation and calculation of transverse distortions due to welding in butt-joints and T-joints. *Welding in the World/Soudage dans le Monde* 34: 397-406.
4. Goglio, L., and Gola, M. M. 1993. Shrinkage in butt-welded joints: Measurements and predictions. *Welding International* 7: 776-787.
5. Tekriwal, P. 1989. Three-dimensional transient thermo-elasto-plastic modeling of gas metal arc welding using the finite element method. PhD dissertation, Urbana, Ill., University of Illinois at Urbana-Champaign.
6. Masubuchi, K. 1980. *Analysis of Welded Structure; Residual Stress, Distortion and their Consequences*. New York, N.Y.: Pergamon Press Inc.
7. Hideyuki, S., and Akitake, M. 1998. Drawbead restraining force when the sliding direction of the sheet is not normal to the drawbead line, a study on drawbead restraining force in sheet metal forming. *Journal of the Japan Society for Technology of Plasticity* 39(448): 33-44.
8. Jang, C. D., and Lee, C. H. 2003. Prediction of welding deformation of ship hull blocks.

Proceedings of International Workshop on Frontier Technology in Ship and Ocean Engineering, pp. 41-49.

9. Ueda, Y., and Ma, N. X. 1995. Measuring methods of three-dimensional residual stresses with aid of distribution function of inherent strains (Report 3). *Transactions of Japanese Welding Research Institute* 24(2): 123-130.

10. Jang, C. D., and Seo, S. I. 1996. A study on the automatic fabrication of welded built-up beams. *Transactions of the Society of Naval Architects of Korea* 33(1): 206-213.

11. Murakawa, H., Luo, Y., and Ueda, Y. 1997. Prediction of welding deformation and residual stress by elastic FEM based on inherent strain. *Journal of the Society of Naval Architects of Japan* 180: 739-751.

12. Seo, S. I., and Jang, C. D. 1999. A study on the prediction of deformations of welded ship structures. *Journal of Ship Production* 15(2): 73-81.

13. Tsai, C. L., Park, S. C., and Cheng W. T. 1999. Welding distortion of a thin-plate panel structure. *Welding Journal* 78(5): 156-s to 165-s.

14. Hoffmeister, H., Harneshaug, L. S., and Roaas, S. 1987. Investigation of the conditions for weld metal hydrogen cracking of low carbon offshore steels by the IRC weldability test. *Steel Res.* 58(3): 134-141.

15. Hoffmeister, H., Christensen, N., and Akselsen, O. M. 1987. Effect of heat input and pre-heating on hydrogen assisted weld joint cracking of a 0.13%C, 1.5%Mn, 0.032%Nb high strength steel of 50 mm plate thickness in the IRC test. *Steel Res.* 58(12): 570-576.

16. Bretz, W., and Hoffmeister, H. 1987. Effect of hydrogen, restraint, and welding conditions on weld metal cold cracking of HSLA Steels in the IRC Test. *Steel Res.* 58 (3): 142-147.

17. Potente, H., Schneiders, J., Herrmann, K. P., Ferber, F., and Linnenbrock, K. 2001. Investigations concerning the development of inherent stresses during welding by using the drilled-hole method as well as the finite element method. *Welding in the World* 45(1/2): 9-17.

18. Boellinghaus, T., and Kannengiesser, T. 2003. Effect of filler material selection and shrinkage restraint on stress strain buildup in component welds. *6th International Trends in Welding Research Conference Proceedings*, ASM International, pp. 906-911.

19. Kannengieber, T., Bollinghaus, T., Florian, W., and Herold, H. 2001. Effect of weld metal strength and welding conditions on reaction forces and stress distribution of restrained components. *Welding in the World* 45(1/2): 18-26.

20. Cornu, Jean. 1988. *Advanced Welding System: Fundamentals of Fusion Welding Technology*. Bedford, UK: IFS publication Ltd.

21. Henrik Runnemalm. 1999. Efficient finite element modelling and simulation of welding. PhD dissertation, Department of Mechanical Engineering, Lulea University of Technology, Lulea, Sweden.